Radiation transport effects and the interpretation of infrared images of gravity waves and turbulence

John Gruninger and James W. Duff
Spectral Sciences, Inc., Burlington, MA

James H. Brown and William A. M. Blumberg
USAF Research Laboratory, Hanscom AFB, MA

ABSTRACT

Radiation transport modulates the spatial frequencies of atmospheric structures, acting as a low pass filter, which causes the power spectra of the accumulated radiance to have different power spectral slopes than the underlying atmospheric structure. Additional effects arise because of the non-stationarity of the atmosphere. The SHARC atmospheric radiance code is used to model both equilibrium and non-equilibrium radiance and radiance fluctuation statistics. It predicts two dimensional radiance spatial covariance functions and power spectral densities, PSDs. Radiance power spectral slopes for paths through isotropic Kolmogorov turbulence are predicted to vary from –5/3 to –8/3 depending on the length of the path through the turbulence. The input gravity wave 3-D covariances and PSDs of atmospheric temperature are consistent with current gravity wave theory, having vertical and horizontal power spectral indices of -3 and –5/3, respectively. Altitude profiles of variances and correlation lengths account for the non-stationary of the gravity wave structure in the atmosphere. The radiance covariance and PSD power spectral slopes differ from the atmospheric gravity wave temperature model values of -3 and –5/3. These modulations depend on LOS orientations, and scale lengths of the sampled altitudes along the LOS.

1. INTRODUCTION

This paper discusses the effects of radiation transport on 3-D atmospheric structures induced by gravity waves and turbulence. The radiance structure of atmospheric backgrounds is induced by local temperature and density fluctuations in the atmosphere. Radiation transport modulates the spatial frequencies of atmospheric structures. The transport acts as a low pass filter, and causes the power spectra of the accumulated radiance to have different power spectral slopes than the underlying atmospheric structure. Additional effects arise because of the non-stationarity of the atmosphere. Horizontal spatial scales of the atmosphere structure grow with altitude. When the structure from several altitude layers contribute to the radiance, several scale lengths are present in the radiance images. Multiple scales can introduce breaks in the radiance power spectral slopes and have the effect of lowering the spectral slope of the composite power law PSD at spatial frequencies between the high and low frequency structures. The Strategic High Altitude Radiance Code (SHARC)[1] calculates mean line-of-sight (LOS) radiance and transmittance values. Its structure

Report Documentation Page

Form Approved
OMB No. 0704-0188

1. REPORT DATE	2. REPORT TYPE	3. DATES COVERED
1998		**00-00-1998 to 00-00-1998**

4. TITLE AND SUBTITLE	5a. CONTRACT NUMBER
Radiation transport effects and the interpretation of infrared images of gravity waves and turbulence	5b. GRANT NUMBER
	5c. PROGRAM ELEMENT NUMBER
6. AUTHOR(S)	5d. PROJECT NUMBER
	5e. TASK NUMBER
	5f. WORK UNIT NUMBER
7. PERFORMING ORGANIZATION NAME(S) AND ADDRESS(ES) **Spectral Sciences Inc,4 Fourth Avenue,Burlington,MA,01803-3304**	8. PERFORMING ORGANIZATION REPORT NUMBER
9. SPONSORING/MONITORING AGENCY NAME(S) AND ADDRESS(ES)	10. SPONSOR/MONITOR'S ACRONYM(S)
	11. SPONSOR/MONITOR'S REPORT NUMBER(S)

12. DISTRIBUTION/AVAILABILITY STATEMENT
Approved for public release; distribution unlimited

13. SUPPLEMENTARY NOTES

14. ABSTRACT

15. SUBJECT TERMS

16. SECURITY CLASSIFICATION OF:			17. LIMITATION OF ABSTRACT	18. NUMBER OF PAGES	19a. NAME OF RESPONSIBLE PERSON
a. REPORT	b. ABSTRACT	c. THIS PAGE			
unclassified	**unclassified**	**unclassified**		**14**	

model[2] predicts the two-dimensional spatial covariance function of the radiance. The covariance function and its Fourier transform, the power spectral density (PSD), can be use directly in sensor models or in image synthesis models[3] to create realizations of the predicted structure. The radiance statistics and images are non-stationary and are explicitly dependent on spectral band pass and sensor field-of-view (FOV). An additional quantity derived by the structure model is a LOS radiance covariance distribution function. The radiance covariance distribution function acts as a weighting function, which reveals the relative importance of temperature and density fluctuations to radiance variance at each location along the LOS. The radiance covariance distribution function also provides the distribution of scales lengths and power spectral slopes. The SHARC model predicts that radiance power spectral slopes depend on LOS orientation and on the relative horizontal to vertical scale lengths that are present in the atmospheric structures. These changes in form of the power spectra must be taken into account when making inferences about the atmospheric structure from the analysis of infrared imagery.

There is considerable evidence for isotropic turbulence in the troposphere[4,5], and for gravity wave structures in the mesosphere[6,7]. Recently, evidence for thunderstorm generated gravity wave structures in infrared images in the upper stratosphere has been reported[8]. The SHARC structure model predicts that radiance power spectral slopes for paths through isotropic Kolmogorov turbulence[9] are modulated to vary from –5/3 to –8/3 depending on the length of the path through the turbulence, differing from the isotropic temperature power spectral slope of –5/3. The effect is similar to the wet delay interference observed in the radio interferometric measurements. These experiments measure the differential phase between two paths. The wet delay is caused by water vapor fluctuations in the troposphere, which induce refractive index fluctuations along the LOS paths. The wet delay has been successfully modeled[4,5] based on isotropic Kolmogorov turbulence. While there has been no reported modulating effects of radiation transport through gravity wave structures, the emission power spectra[6] of O_2 airglow and of the OH airglow[7] appear to be steeper than the simultaneously measured rotational temperature power spectra. SHARC contains a non-isotropic gravity wave power law model. The predicted radiance PSD power spectral slopes differ from the power law temperature and density fluctuation models. The modulations are shown to depend on LOS orientation and on the relative scale lengths along the LOS.

2. RADIANCE STRUCTURE CALCULATION TECHNIQUE

The SHARC model[1] calculates mean LOS radiance and transmittance values. Its structure model[2] predicts the two-dimensional spatial covariance function of the radiance and a radiance covariance distribution function. The covariance function and its Fourier transform, the power spectral density (PSD), can be use directly in sensor models or in image synthesis models[3] to create realizations of the predicted structure. The radiance statistics and images are non-stationary and are explicitly band pass and sensor FOV dependent. The inputs to the calculation are altitude dependent temperature and density profiles, which can be obtained from the standard atmosphere generator (SAG)[10] model and an atlas of molecular line parameters based on HITRAN-92.[11] The non-stationary altitude dependence of the temperature fluctuations are modeled by profiles of temperature variance and horizontal and vertical correlation lengths. Current estimates of these profiles are taken from the non-stationary stochastic (NSS) model.[12] In the troposphere and stratosphere collisional quenching of excited vibrational states is fast compared to radiative decay. Species tend to be in local thermodynamic equilibrium (LTE). Above the stratosphere, there are an

insufficient number of collisions to equilibrate vibrational energy before radiative decay occurs. The vibrational states are not characterized by the kinetic temperature. Under these conditions, the vibrational states are in non-local thermodynamic equilibrium (NLTE). SHARC contains NLTE models for both mean properties, radiances and transmittances, and for the fluctuation responses. Under NLTE conditions, the response of population changes to fluctuations in temperature and density are determined for each state by a perturbation model which uses the same steady state chemical-kinetics schemes that are used for the quiescent atmosphere. Fluctuations in the kinetic temperature can result in correlated or anti-correlated responses in vibrational state population. The magnitudes of the responses depend on the local chemical-kinetics environment. NLTE emission depends on the vibrational temperatures of all species involved, as well as, the kinetic temperature. The starting point for determining the radiance covariance is a radiance fluctuation expressed as the accumulation of responses to local atmospheric fluctuations in temperature[2]

$$\Delta L_{\Delta\lambda}(\vec{p}) = \int dr F_{\Delta\lambda}(\vec{r})\Delta T(\vec{r})\,. \qquad \textbf{(1)}$$

$F_{\Delta\lambda}(\vec{r})$ includes radiance fluctuation contributions induced by the rearrangement of population among the molecular vibrational states, $F^{j}_{\Delta\lambda}(\vec{r})$ and kinetic temperature fluctuations, $F^{o}_{\Delta\lambda}(\vec{r})$,

$$F_{\Delta\lambda}(\vec{r}) = \sum_{j} F^{j}_{\Delta\lambda}(\vec{r})\partial T^{j}_{vib}(\vec{r})/\partial T(\vec{r}) + F^{o}_{\Delta\lambda}(\vec{r})\,. \qquad \textbf{(2)}$$

The radiance covariance $Cov_L(\vec{p},\vec{p}\,')$, where $\vec{p}$ and $\vec{p}\,'$ point to two locations in the sensor image, can be expressed as

$$Cov_L(\vec{p},\vec{p}\,') = E\left[\Delta L_{\Delta\lambda}(\vec{p})\Delta L_{\Delta\lambda}(\vec{p}\,')\right] \qquad \textbf{(3)}$$

E[x] is the expectation value of x. Substituting Equation (1) into Equation (3) yields

$$Cov_L(\vec{p},\vec{p}\,') = \int dr \int dr' F_{\Delta\lambda}(\vec{r})F_{\Delta\lambda}(\vec{r}\,')Cov_T(\vec{r},\vec{r}\,') \qquad \textbf{(4)}$$

It is assumed that the radiance covariance and the 3-D atmospheric temperature covariance are locally stationary. Under this assumption, within a region about a pixel, $\vec{p}$, in the sensor image, the radiance covariance only depends on the lag, $\Delta\vec{p} = \vec{p} - \vec{p}\,'$. Likewise, within the atmosphere the temperature covariance is only a function of the lag, $\Delta\vec{r} = \vec{r} - \vec{r}\,'$, about the point $\vec{r}$.

A useful intermediate quantity results from the integration over the LOS r'. The result is function of position along the reference LOS, and describes the distribution of contributions of the atmospheric structure to the radiance covariance. The resulting radiance covariance distribution function determines the LOS spatial distribution of the radiance covariance. For a particular

location along the central LOS, the integration over all points along the second LOS r' is equivalent to integration over all lags, $\Delta\vec{r}$, equal to or larger than the minimum lag at the point, $\Delta\vec{r}_{\amalg}$. The minimum lag between the two LOS is parallel to the lag vector, $\Delta\vec{p}$, in the image plane, as illustrated in Figure 1. The radiance covariance is given by

$$\mathrm{Cov_L}(\vec{\mathrm{p}}, \Delta\vec{\mathrm{p}}) = \int \mathrm{drW_L}(\vec{\mathrm{r}}, \Delta\vec{\mathrm{r}}_{\amalg}) \qquad \textbf{(5)}$$

where the radiance covariance distribution function, $\mathrm{W_L}(\vec{\mathrm{r}}, \Delta\vec{\mathrm{r}}_{\amalg})$, is defined as

$$W_L(\vec{r}, \Delta\vec{r}_{\amalg}) = \int dr' F_{\Delta\lambda}(\vec{r}) F_{\Delta\lambda}(\vec{r}') Cov_T(\vec{r}, \Delta\vec{r}) . \qquad \textbf{(6)}$$

When the lag in the image is zero, the minimum lag along the LOS, $\Delta\vec{r}_{\amalg}$, is also zero . Integration of Equation (5) for zero lag leads to a LOS variance distribution function, or weighting function, $W_L(\vec{r},0)$. The radiance variance is given by

$$\sigma_L^2(\vec{p}) = \int dr W_L(\vec{r},0) . \qquad \textbf{(7)}$$

The variance distribution function determines how contributions to the radiance structure are distributed along the LOS through the atmosphere. The integrations over the two LOS through the 3-D atmosphere cause changes in the form of the radiance covariance function relative to the temperature covariance, typically yielding a different spatial frequency dependence. These changes are consequences of the non-separability and non-stationarity of the temperature covariance along the LOS. In the next subsection we focus on the first integration and the nature of the resulting radiance covariance distribution function. In the subsequent section we illustrate the effects of non-stationarity in the process of evaluating the radiance covariance by integrating the radiance covariance distribution function.

3. EVALUATION OF THE RADIANCE COVARIANCE DISTRIBUTION FUNCTION

In this section, we consider several limiting cases of the radiance covariance distribution function. First, a special case of a single narrow layer of structure is considered. Second, an isotropic temperature covariance, which is relevant to the isotropic turbulence situation, is considered. Finally, the case of non-isotropic structures is considered, using a temperature covariance model that describes gravity wave structure in the atmosphere.

3.1 Very narrow altitude layers of structure

If the structure is dominated by a single narrow altitude layer, the integrand in Equation 5 may remain approximately constant. If the radiators in the band pass are present only in a narrow altitude layer, then $F_{\Delta\lambda}(\vec{r}')$ is zero except for a short segment of the LOS, Δs, located at the center of the layer, r_o. The integral in Equation 5 can then be approximated by

$$W_L(\vec{r}_0, \Delta\vec{r}_{\text{II}}) \approx \Delta s F_{\Delta\lambda}^2(\vec{r}_0) Cov_T(\vec{r}_0, \Delta\vec{r}_{\text{II}}) \quad \textbf{(8)}$$

In this approximation, the radiance distribution function is non-zero only at the same altitude layer as the temperature fluctuation and the radiance covariance is given by

$$Cov_L(\vec{p}, \Delta\vec{p}) \approx \Delta s W_L(\vec{r}_0, \Delta\vec{r}_{\text{II}}) \quad \textbf{(9)}$$

The resulting radiance covariance is equal to the atmospheric temperature covariance in the direction parallel to the image plane. The conditions for this to be valid are rather stringent. The path of the LOS through the layer, Δs, must be short compared to the correlation length of the temperature structure along the LOS, in order for the temperature covariance to be constant in the LOS direction. This will become more apparent when paths through isotropic and general non-separable structures are analyzed.

3.2 Isotropic temperature structure

The second special case is that of an isotropic temperature covariance. This is important for describing isotropic turbulence structures in the low altitude and boundary layer. To simplify the analysis we use an approximation suggested by Lindquist, Kwon, and Nagy.[13] If the radiance fluctuation amplitude is a slowly varying function of location along the LOS, the product $F_{\Delta\lambda}(\vec{r}) F_{\Delta\lambda}(\vec{r}\,')$ can be replaced by the square of the radiance fluctuation amplitude, $F_{\Delta\lambda}^2(\vec{r})$, at $\vec{r}$ and taken outside of the integral in Equation 5, resulting in

$$W_L(\vec{r}, \Delta\vec{r}_{\text{II}}) \approx F_{\Delta\lambda}^2(\vec{r}) \int dr' Cov_T(\vec{r}, \Delta\vec{r}) \,. \quad \textbf{(10)}$$

This is just the opposite of the narrow layer approximation made above. Since the temperature covariance is isotropic, its dependence on the lag is independent of direction and is only a function of the magnitude of the lag, $|\Delta\vec{r}| = \sqrt{\Delta x^2 + \Delta y^2 + \Delta z^2}$. If we let the image plane be the XY plane, the lag $, \Delta r_{\text{II}}$, whose magnitude is $|\Delta r_{\text{II}}| = \Delta\rho = \sqrt{\Delta x^2 + \Delta y^2}$,is also in the XY direction. and the LOS integration is along z. The covariance is not separable along the LOS and the resulting covariance distribution is modified in the XY plane. As an example, a simple exponential covariance function with unit variance and scale length, $Cov_T = e^{-|\Delta r|}$, can be integrated to give

$$W_L(\vec{r}, \Delta\rho) = F_{\Delta\lambda}^2(\vec{r}) \int dz e^{-|\Delta r|} = F_{\Delta\lambda}^2(\vec{r}) \rho K_1(\rho) \quad \textbf{(11)}$$

where K_1 is a modified Bessel function of the second kind of order 1. Integration through the isotropic 3-D covariance yields an isotropic covariance distribution function, but it is not exponential. The integral can be found in compendiums of integrals of Bessel functions[14]. The exponential can also be expressed as $e^{-r} \Rightarrow r^{1/2} K_{1/2}(r)$. The general result of the integration in Equation 10 is to produce a new Bessel function whose order is increased by 1/2. These functions are the covariance functions of the power law PSD's. If η is the order of the Bessel function, then the corresponding power law PSD has the form $(1 + \mathrm{k}^2)^{-(\eta+1/2)}$ which in the high frequency limit $\Rightarrow k^{-2\eta+1}$. In the exponential example, the power law spectral index changed on integration from -2 for the exponential to -3 for the radiance covariance distribution function. In general, a change in

order of Bessel function by one half corresponds to a change in spectral index of minus one. If one uses a simple Kolmogorov turbulence model[9] of spectral index -5/3, the integration leads to a radiance covariance distribution function with a spectral index of -8/3. This is also the basis for the theoretical findings in the wet delay modeling of radar interferometry.[4,5] A caveat is that the analytical integrations are over all space. To determine the actual length of the path that is required for modulation, the integration was performed numerically for a grid of interval widths from zero to several scale lengths. The results of these integrations are shown in Figure 2. The results for the simple exponential case are instructive for other power law covariances. The covariance distribution is modified almost completely for all lags that are on the order of the length of the path through the structure. After the path length is longer than a few scale lengths, the covariance distribution is essentially of the next highest half order over its measurable range. This confirms that the only time that the approximation in Section 3.1 is valid is for lags and temperature covariance scale lengths that are large compared to the path length through the structure. In addition to changes in spectral slope, the integration leads to a change in correlation length. For the simple exponential, the scale length and the correlation length are the same. However, for the modified Bessel function covariances of order, *0*, the correlation length is equal to $C_l = \sqrt{\Pi}\,\Gamma(\eta+1/2)/\Gamma(\eta)$ where э is the gamma function. In Figure 2b the correlation length increases from 1 for the exponential covariance to a correlation length of B/2 as the path through the layer increases. The integral in Equation 5 can only be replaced by the integrand times the path length of the LOS through the narrow region for lags larger than the path length through the structure and for temperature correlation lengths in the LOS direction that are longer than the path through the layer.

It is instructive to evaluate the integral in Equation 10 using Fourier techniques. Expressing the 3-D temperature covariance in terms of its 3-D PSD yields

$$\int \mathrm{dz}\mathrm{Cov}_T(\vec{\mathrm{r}},\Delta\mathrm{r}) = \int \mathrm{dz}\int \mathrm{dk}_z \mathrm{e}^{-\mathrm{ik}_z z}\int \mathrm{dk}_x \mathrm{e}^{-\mathrm{ik}_x x}\int \mathrm{dk}_y \mathrm{e}^{-\mathrm{ik}_y y}\mathrm{PSD}_{3-D}(\sqrt{\mathrm{k}_z^2+\mathrm{k}_x^2+\mathrm{k}_y^2}) \qquad (12)$$

Integrating first over *dz* yields a Dirac delta function[15] $\delta(k_z)$ in spatial frequency along the LOS direction, z. The result is

$$W_L(\vec{r},\Delta\rho) \Rightarrow \int dzCov_T(\vec{r},\Delta r) = \int dk_x e^{-ik_x x}\int dk_y e^{-ik_y y} PSD_{3-D}(\sqrt{k_x^2+k_y^2}). \qquad \mathbf{(13)}$$

The integration through the 3-D temperature covariance along a LOS yields a 2-D radiance covariance. The 2-D covariance is the Fourier transform pair of the 3-D PSD with zero spatial frequency in the LOS direction.

In the special case of the Komogorov isotropic turbulence model , for example, the 1-D, 2-D and 3-D power law spectral indices are –5/3, -8/3, and –11/3, respectively. The 2-D temperature PSD is obtained from the 3-D temperature PSDby integrating over all of the spatial frequencies in the third dimension. The summing over all spatial frequencies in the third dimension leads to the 2-D temperature PSD with its larger spectral index. The effects of the LOS integration is to remove all high frequencies in the third dimension. LOS integration generates a 2-D radiance PSD with the 3-D temperature spectral indices. The radiance covariance distribution function for the Komogorov turbulence has a 2-D spectral index of –11/3 and a 1-D index of –8/3. The 2-D spatial frequency distribution observed in the image plane is the 3-D spatial frequency distribution of the atmosphere in that plane for zero spatial frequencies along the LOS The LOS integration eliminates the 3-D

spatial structures that are correlated with high spatial frequencies along the LOS. What is retained in the image plane is the accumulation of the high and low spatial frequency structures, which are correlated to the low spatial frequencies in the LOS direction . It is the selective retention of the low spatial frequency structure in the LOS direction that causes selectiveness in the image plane when the LOS direction in the 3-D covariance is non-seperable from image plane. Equations 12 and 13 above show that the low pass filtering properties of radiation transport is general and not restricted to power law models.

3.3 Non-Isotropic Gravity wave Model

The power law temperature covariance model contained in SHARC is consistent with current gravity wave models. At any point, $\vec{r}$, along the LOS the temperature covariance is assumed to be separable into horizontal, ρ ,and vertical ,z, components

$$Cov_T(\vec{r},\Delta\vec{r}) = Cov_H(\vec{r},\Delta\rho)Cov_V(\vec{r},\Delta z)\,. \qquad \textbf{(14)}$$

The vertical component has a spectral index of –3. The 2-D horizontal covariance is taken to be isotropic with a one dimensional spectral index of –5/3. There are two special situations which arise in the evaluation of the radiance covariance distribution which can be analytically determined. We utilize approximations which are not made in the SHARC model, to simplify the analysis and provide insight into the results generated by the more accurate model. For long range nadir or zenith viewing, where the LOSs are approximately parallel and vertical, the LOS integrations are in the vertical direction . In this situation, the horizontal covariance does not depend on the integration variable , the vertical altitude lag, Δz , and Equation 5 can be approximated for nadir/zenith viewing

$$W_L(\vec{r},\Delta\vec{r}_{\amalg}) \approx W_L(z,\Delta\rho) = Cov_H(z,\Delta\rho)\int d(\Delta z)F^2_{\Delta\lambda}(z)Cov_V(z,\Delta z) = Cov_H(z,\Delta\rho)\omega(z)\,. \qquad \textbf{(15)}$$

The integration over the altitude lag leads to an altitude weighting, $\omega(z)$, of the horizontal covariance. This is a different result from the isotropic case, since the radiance variance distribution has the same power spectral slope and correlation length as the horizontal temperature covariance at the altitude z. Unlike the situation for isotropic turbulence, nadir views through the separable gravity wave model would have a PSD with spectral slope close to -5/3. While the same bias toward low frequency structure in the LOS direction exists in both models, by being separable the horizontal spatial frequencies are unaltered by the bias.

Another approximate situation occurs if the LOS is in the horizontal. In the case of horizontal viewing, ignoring earth curvature, the LOS path is through the horizontal isotropic structure and the vertical temperature covariance can be factored out of the integral resulting in the radiance covariance for horizontal viewing

$$W_L(x,\Delta y,\Delta z) = F^2_{\Delta\lambda}(x)Cov_V(x,\Delta z)\int d(\Delta x)Cov_H(x,\Delta\rho) = \omega(x)Cov_V(x,\Delta z)\overline{C}ov_H(x,\Delta y)\,. \quad \textbf{(16)}$$

Here the x axis is taken to be the horizontal direction for the LOS. Since the temperature covariance is separable , the radiance covariance distribution function is also separable with a vertical component which is not modulated with a power spectral index of -3 and an unchanged correlation length. The horizontal component is modulated by the LOS integration through the 2-D isotropic structure. The radiance covariance distribution horizontal power spectral slope is modified from –5/3 to –8/3, and its correlation length is increased over the atmospheric temperature values. Also within the flat earth approximation. The radiance covariance distribution vertical power spectral slope would equal -3. The flat earth approximation is severe and the actual treatment of limb views is reserved for the general case.

The path integration effects for general viewing geometries have to be evaluated numerically. The integrations are performed using the SHARC structure model. Within this model, LOS's are diverging, based on the observer and structure geometry. The model assumes a spherical earth. Furthermore, the fluctuation amplitudes are included in the integrations so that no assumptions are needed about their constancy, that is SHARC numerically integrates Equation 5. Based on the results of the special cases, we can anticipate that the radiance covariance distribution function will have a different functional form from the 3-D temperature covariance, and that the changes will be a function of the LOS angle through the structure. In addition, there are strong effects based on the ratio of horizontal to vertical correlation lengths. The radiance covariance distribution function was evaluated for a 35 km thick layer of structure between 30 and 65 km in altitude for a grid of ratios of temperature correlation lengths. The sensor was placed above the structure and its look angles changed so that several local off nadir angles could be sampled. The covariance distribution function was evaluated at 40km. The local off nadir angle is the intersection angle of the LOS with the structure at 40km. The radiance power spectral slopes changes for horizontal to vertical temperature correlation length ratios of 1, 5, and 20 are reported in Figure 3. For all correlation length ratios the radiance covariance distribution power spectral slopes are within -1.66 to -1.8 at nadir viewing. Here, the sensor vertical and horizontal are parallel to the earth. When the viewing is nearly horizontal the sensor vertical is perpendicular to the earth and the power spectral slopes of radiance covariance distribution function are close to the -8/3 and -3 for the horizontal and vertical, respectively, as predicted by the approximate model. For intermediate local off-nadir angles the behavior is a function of the correlation length ratios. For large horizontal to vertical ratios, the sensor vertical spectral slope is close to -4 for a range of almost 60^o between 30^o and 90^o off-nadir angles, the vertical slope rapidly falls off toward -5/3 as the sensor vertical points more and more into the atmospheric horizontal direction. The horizontal power spectral slope is very close to -2 over almost the entire range of off nadir angles, except for the limb and nadir. When the ratio for temperature correlation lengths is 1, the sensor vertical spectral slope has a narrow minimum of about -3.5 at 60 to 70 degrees off nadir while the horizontal spectral slope is close to -8/3 from 60 to 90 and steeper than -2 for almost all off-nadir viewing angles. These grids represent the anticipated range of values of power spectral slopes that may be measured that is consistent with the gravity wave power law model.

4. RADIANCE COVARIANCE

The final step in determining the radiance covariance is the second LOS integration, ie that of integrating the radiance covariance distribution along the LOS. If the LOS is for limb viewing, and the radiance covariance distribution function is dominated by a single altitude layer with a single set of correlation lengths, the radiance covariance will be proportional to the radiance covariance distribution function at that altitude. The integration of the radiance covariance distribution function can dramatically alter the shape of the radiance covariance function when different scales are involved. The non-stationarity of the atmospheric structure can lead to a radiance covariance distribution function that has widely different correlation lengths at different ranges or altitudes along the LOS. If there are significant contributions from altitudes with different correlation lengths, the integrations can lead to breaks in the spectral slope of the radiance covariance and to shallow spectral slopes at spatial frequencies between the largest and smallest scales. An example of the effect is illustrated in Figure 4, in which two PSD's with the same spectral index of -8/3, but with correlation lengths of 4 km and 40 km are added together. The blend has a break at the roll over point of the shorter correlation length PSD. The blend has a shallow spectral slope until the 40km PSD dominates at lower frequencies. The production of frequency regions of shallow spectral slope has been used by the image syntheses community to generate pseudo fractal scenes from simple auto regressive processes.[16] Short range viewing of structure of constant scale lengths can exhibit the same effects because structure in the near field will appear larger than structure at a distance. The effects of non-parallel LOS's in the FOV generates covariance distribution functions with apparent correlation lengths that are large in the near field and smaller at long range even for actual temperature structure which is stationary.

4.1 Example BTH off Nadir FOV for $CO_2(\nu_3)$

The Midcourse Space Experiment (MSX) has collected a large quantity of IR imagery in narrow bands around the heart of the 4.3 :m CO_2 band. The data includes low altitude limb views, below the horizon views, and nadir scenes. These data should provide a wealth of information on the atmospheric structures present between 20 km and 60 km in altitude. To illustrate the predictions of the forward model, calculations were performed for the narrow 4.22-4.36 :m band for a LOS close to the horizon, sensor off nadir angle of 59 degrees. The covariance distribution function was numerically calculated and profiles of its variance, local correlation lengths and power spectral slopes were determined. These profiles are reported in Figure 5. The horizontal power spectral slope varies from about -7/3 at the higher altitudes to -8/3 at 20 km, while the sensor vertical slope varies from -4 at the higher altitudes to -3.3 at 20 km. This reflects the behavior described above of large versus small temperature horizontal to vertical correlation length ratios. The radiance covariance distribution function horizontal and vertical correlation lengths reflect the continuous increase in scale lengths with altitude described by the quiescent input temperature model profiles. The variance distribution shows the altitude weighting of the covariance distribution functions contribution to the radiance covariance. The radiance covariance function was computed and its properties determined. The relative standard deviation (sigma/mean) of 5%, sensor horizontal and vertical correlation lengths of 11.7 km and 2 km, respectively and horizontal and vertical spectral slopes of -2.2 and -3.6, respectively, were determined. The horizontal power spectral slope of -2.2 reflects the effects of

accumulation of contributions over several correlation lengths. It is smaller than any single local contribution of the radiance covariance distribution function. A comparison of the numerical covariance versus the analytical power law function computed over a range of 50 km shows no breaks or any significant deviations over that range. This is the range of continuous correlation length changes in the quiescent NSS temperature statistics profiles.

5. CONCLUSIONS

The radiance structure of atmospheric backgrounds is induced by local temperature and density fluctuations in the atmosphere. Radiation transport effects modulate the spatial frequencies of atmospheric structures, acting as a low pass filter, which modifies power law spectral slopes. The non-stationarity of the atmosphere causes structure of several scales to be in the FOV. This is expected to be particularly prevalent whenever several altitude layers contribute strongly to the covariance distribution. Multiple scales can introduce breaks in the power law spectra and lead to shallower spectral slopes of the composite power law PSD at spatial frequencies between the high frequency and low frequency structures in the FOV. The importance of various altitude contributions along the LOS can be assessed by the variance distribution function. The radiance power spectral slopes depend on LOS zenith angles and on the relative horizontal to vertical scale lengths that are present in the atmospheric structures. These effects must be taken into account when making inferences about the atmospheric structure from analysis of infrared imagery.

6. ACKNOWLEDGMENTS

This work sponsored by Ballistic Missile Defense Organization under Air Force Contract No. F19628-91-C-0083. The authors are grateful to Drs. Ramesh Sharma and Laila Jeong (AF Research Laboratory) for continuing support and interest in this work.

7. REFERENCES

1. R. L. Sundberg, J. W. Duff, J. H. Gruninger, L. S. Bernstein, M. W. Matthew, Adler-Golden, D. C. Robertson, R. D. Sharma, J. H. Brown, and R. J. Healey, "SHARC, A Model for Calculating Atmospheric Infrared Radiation Under Non-Equilibrium Conditions," in *The Upper Mesosphere and the Lower Thermosphere: A Review of Experiment and Theory, Geophysical Monograph Series*, **87**, 287-295, 1995.
2. J. Gruninger, R. L. Sundberg, J. W. Duff, J. H. Brown, R. D. Sharma, and R. D. Sears, "Modeling Atmospheric Background Radiance Structures," *SPIE proceedings European Symposium on Satellite Remote Sensing II*, **2580**, 1-16, 1995.
3. J. H. Brown and N. J. Grossbard, "Fast 'stretched-space' method for generating synthetic vertical sheets of non-stationary stochastic atmospheric structure for infrared background scene simulations," *Optical Engineering*, **35**, 1035-1043, 1996.

4. R. N. Treuhaft and G. E. Lanyi, "The effect of the dynamic wet troposphere on radio interferometric measurements," *Radio Science*, **22**, 251-265, 1987.

5. C. S. Ruf and S. E. Beus, "Retrieval of tropospheric water vapor scale height from horizontal turbulence structure," *IEEE Trans. Geoscience and Remote Sensing*, **35**, 203-211, 1997.

6. R. H. Weins, D. Y. Wang, R. N. Pertson, and G. G. Shepherd, "Statistics of gravity wave seen in O2 nightglow over Bearlake Observatory," *J. Geophys. Res.*, **102**, 7319-7329, 1997.

7. E. M. Dewan, "An Investigation of the causes of optical and infrared airglow structures in the atmosphere," PL-TR-94-2261, Phillips Laboratory, Hanscom AFB, Mass, October, 1994.

8. E. M. Dewan, R. H.Picard, R.R. O'Neil, H.A. Gardner , J. Gibson, J.D. Mill, E.Richards, M. Kendra, W. O. Gallery, "MSX satellite observations of thunderstorm-generated gravity waves in mid-wave infrared images of the upper stratosphere," *Geophys. Res. Letters*, **25**, 939-942, 1998.

9. V. I. Tatarski, "Wave propagation in a Turbulent Medium," Dover, New York, 1961.

10. S. M. Adler-Golden, "Description of the SHARC Atmosphere Generator," PL-TR-93-2123, Phillips Laboratory, Hanscom AFB, Mass, May 1993.

11. L. S. Rothman, R. R. Gamache, A. Goldman, L. R. Brown, R. A. Toth, H. M. Pickett, R. L. Poynter, J.-M. Flaud, C. Camy-Peyret, A. Barbe, N. Husson, C. P. Rinsland, and M. A. H. Smith, "The HITRAN Molecular Database: Editions of 1991 and 1992," *J. Quant. Spectrosc. Radiat. Transfer*, **48**, 469, 1992.

12. L. A. Strugala, R. D. Sears, J. E. Newt, and B. J. Herman, "Production of Statistically Nonstationary Stochastic Structure Realizations for Infrared Background Scene Simulations," *Optical Engineering*, **32**, 993-1000, 1993.

13. G. H. Lindquist, H. Kwon, and A. R. Nagy, Jr., "Model for Atmospheric Clutter as Seen From a Satellite Platform," *SPIE Proceedings of the Infrared Technology Conference*, **430**, 24-31, 1983.

14. Y. L. Luke, "Integrals of Bessel Functions," McGraw-Hill, New York, 1962.

15. M. J. Lighthill, "Introduction to Fourier Analysis and Generalized Functions," Cambridge University Press, 1964.

8. FIGURES

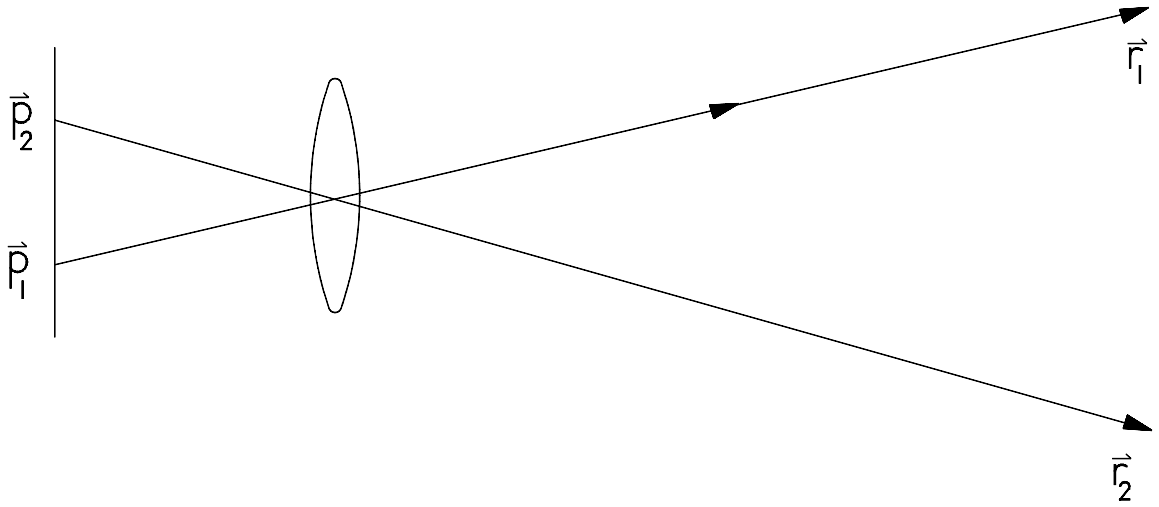

Figure 1. **Two lines-of-sight illustrating the calculation of the radiance covariance distribution function and the radiance covariance.**

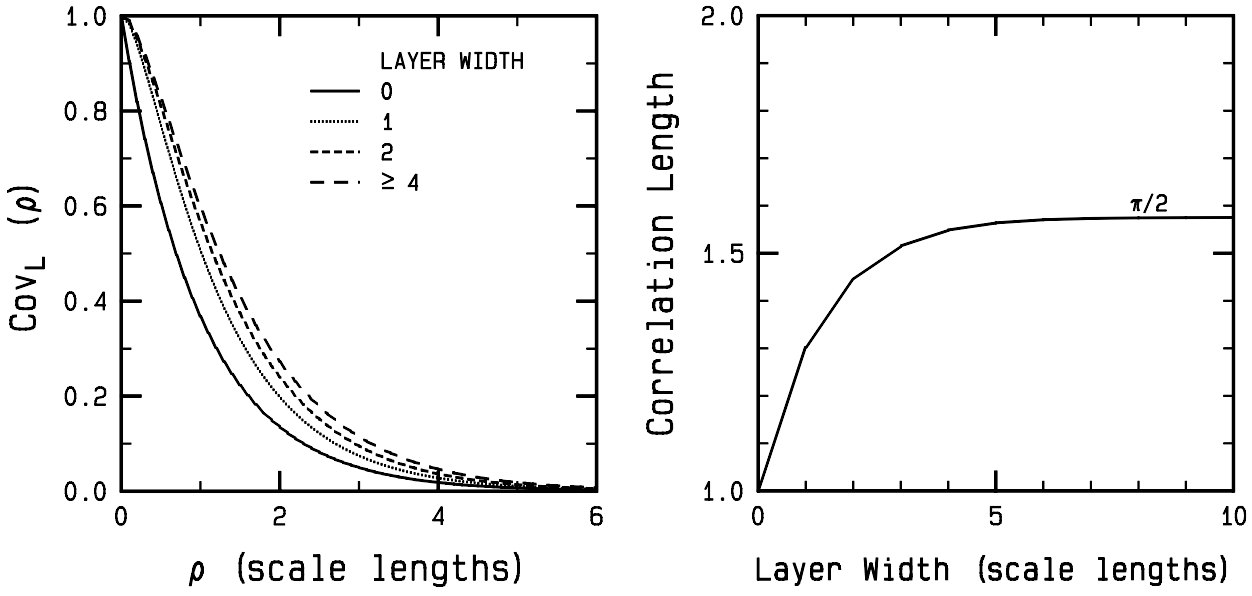

Figure 2. **Covariance distribution functions (left figure) as a function of normalized lag for several layers widths and correlation lengths (right figure) as a function of LOS layer width for isotropic structure.**

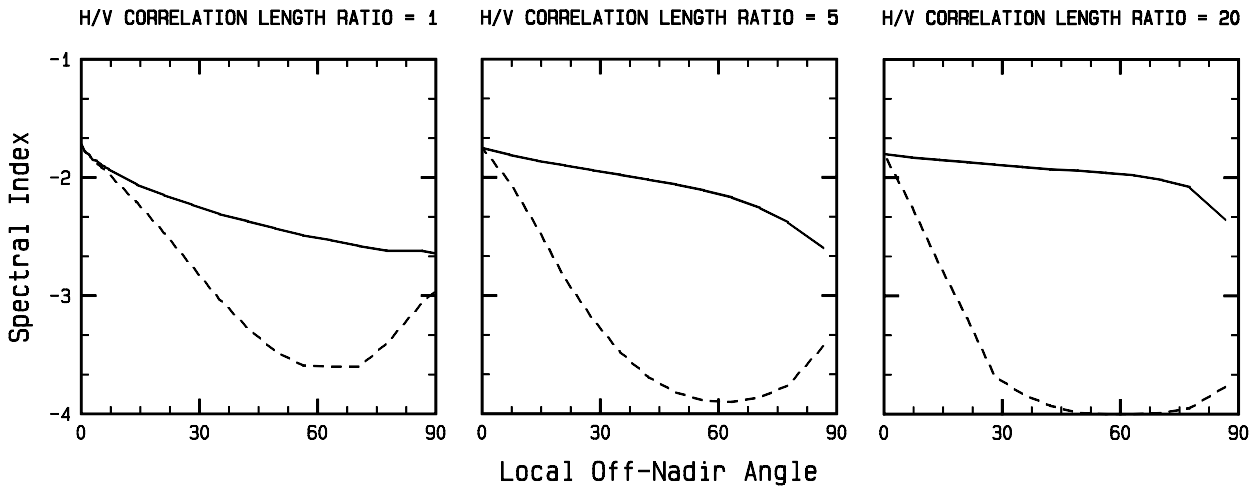

Figure 3. **Angular dependence of the spectral index for several ratios of the horizontal to vertical correlation lengths for sensor horizontal (solid line) and vertical (dashed line).**

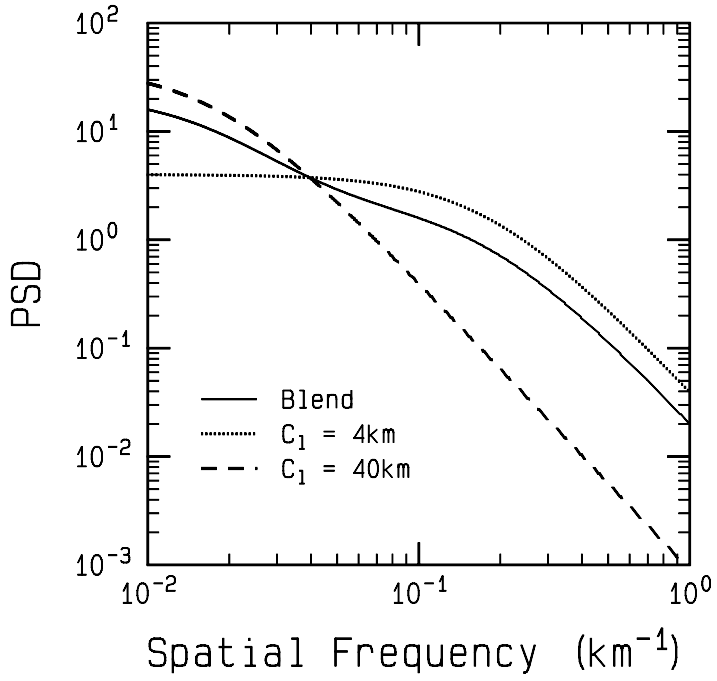

Figure 4. **Generation of shallow power spectral density slopes and breaks from multiple scale structures.**

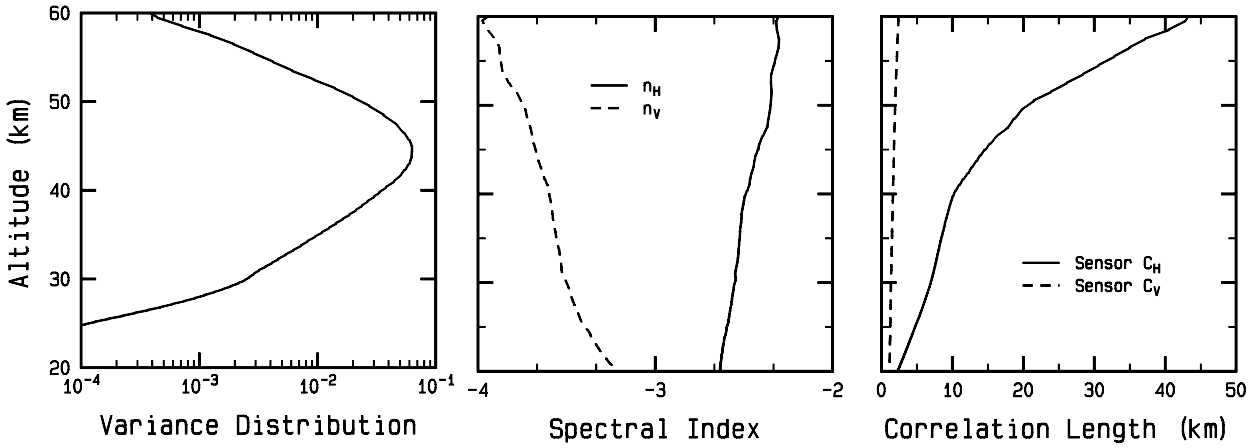

Figure 5. **Altitude dependence of the covariance distribution properties in the MSX band B1 for 59^o off-nadir viewing geometry.**